

# THE JOURNAL OF PHYSICAL CHEMISTRY C

Subscriber access provided by Brought to you by ST ANDREWS UNIVERSITY LIBRARY

C: Energy Conversion and Storage; Energy and Charge Transport

## Exciton-Polaron Interactions in Polyfluorene Films With $\pi$ Phase

Francisco Montilla, Arvydas Ruseckas, and Ifor David William Samuel

*J. Phys. Chem. C*, **Just Accepted Manuscript** • DOI: 10.1021/acs.jpcc.8b01300 • Publication Date (Web): 12 Apr 2018

Downloaded from <http://pubs.acs.org> on April 13, 2018

### Just Accepted

“Just Accepted” manuscripts have been peer-reviewed and accepted for publication. They are posted online prior to technical editing, formatting for publication and author proofing. The American Chemical Society provides “Just Accepted” as a service to the research community to expedite the dissemination of scientific material as soon as possible after acceptance. “Just Accepted” manuscripts appear in full in PDF format accompanied by an HTML abstract. “Just Accepted” manuscripts have been fully peer reviewed, but should not be considered the official version of record. They are citable by the Digital Object Identifier (DOI®). “Just Accepted” is an optional service offered to authors. Therefore, the “Just Accepted” Web site may not include all articles that will be published in the journal. After a manuscript is technically edited and formatted, it will be removed from the “Just Accepted” Web site and published as an ASAP article. Note that technical editing may introduce minor changes to the manuscript text and/or graphics which could affect content, and all legal disclaimers and ethical guidelines that apply to the journal pertain. ACS cannot be held responsible for errors or consequences arising from the use of information contained in these “Just Accepted” manuscripts.



ACS Publications

is published by the American Chemical Society, 1155 Sixteenth Street N.W.,  
Washington, DC 20036

Published by American Chemical Society. Copyright © American Chemical Society.  
However, no copyright claim is made to original U.S. Government works, or works  
produced by employees of any Commonwealth realm Crown government in the course  
of their duties.

1  
2  
3  
4  
5  
6  
7  
8  
9  
10  
11  
12  
13  
14  
15  
16  
17  
18  
19  
20  
21  
22  
23  
24  
25  
26  
27  
28  
29  
30  
31  
32  
33  
34  
35  
36  
37  
38  
39  
40  
41  
42  
43  
44  
45  
46  
47  
48  
49  
50  
51  
52  
53  
54  
55  
56  
57  
58  
59  
60

# Exciton-Polaron Interactions in Polyfluorene Films with $\beta$ Phase

*Francisco Montilla\*<sup>a</sup>, Arvydas Ruseckas<sup>b</sup>, Ifor D.W. Samuel\*<sup>b</sup>*

<sup>a</sup> Instituto Universitario de Materiales de Alicante y Departamento de Química Física

Universidad de Alicante, Apdo. de Correos 99, Alicante 03080, Spain

E-mail: francisco.montilla@ua.es

<sup>b</sup> Organic Semiconductor Centre, SUPA, School of Physics and Astronomy

University of St. Andrews, St. Andrews KY16 9SS, UK

E-mail: idws@st-andrews.ac.uk

1  
2  
3 ABSTRACT  
4  
5

6 Fluorescence quenching by electric charges is an important loss mechanism in high-  
7 brightness organic light emitting diodes (OLEDs) but its effect is difficult to quantify in  
8 working devices. Here we combine an electrochemical technique to control the charge density  
9 with time-resolved photoluminescence to distinguish between different quenching  
10 mechanisms. The material studied was the blue electroluminescent polymer poly(9,9-  
11 dioctylfluorene) with  $\beta$  phase. Our results show that quenching occurs by Förster resonance  
12 energy transfer and is mediated by exciton diffusion. We determine the quenching parameters  
13 over a wide range of charge concentrations and estimate their impact on the OLED efficiency  
14 roll-off at high current density. We find that fluorescence quenching by charges and singlet-  
15 triplet exciton annihilation are the two main mechanisms leading to the efficiency roll-off.  
16 Our results suggest that hole polarons are not very effective quenchers of singlet excitons  
17 which is important for understanding current devices and encouraging for the development of  
18 high-brightness OLEDs and lasers.  
19  
20  
21  
22  
23  
24  
25  
26  
27  
28  
29  
30  
31  
32  
33  
34  
35  
36  
37  
38  
39  
40  
41  
42  
43  
44  
45  
46  
47  
48  
49  
50  
51  
52  
53  
54  
55  
56  
57  
58  
59  
60

## 1. INTRODUCTION

Organic light-emitting diodes (OLEDs) are now used in active-matrix displays of many mobile phones and an increasing number of televisions. The development of other applications, such as solid-state lighting, outdoor displays or window-integrated transparent devices, requires much higher brightnesses and hence much higher current density.<sup>1-4</sup> Device efficiency decreases at high current density, making it important to understand the processes that contribute to this decrease, including luminescence quenching by charges.<sup>5,6</sup> This is particularly relevant to the development of electrically pumped lasers as well as the applications mentioned above.

For highest brightnesses fluorescent materials are used, and we study poly[9,9-dioctylfluorenyl-2,7-diyl] (PFO) as the prototypical example of a blue fluorescent emitter. Bright OLEDs have been reported using PFO with a small amount of planar conformation, the so called  $\beta$  phase.<sup>7-9</sup> These OLEDs show good efficiency of over 3 cd/A at low brightness of 200 cd/m<sup>2</sup> but their efficiency decreases by a factor of two at a brightness of 4000 cd/m<sup>2</sup>. Because the absorption spectrum of injected charges overlaps with the emission spectrum of the polymer, charges can quench light emitting excitons by long-range Förster resonance energy transfer (FRET).<sup>10-13</sup> Besides injected charges, triplet excitons can also quench light emission in OLEDs. Hence, in order to improve the device performance it is important to understand losses at high current density. Fluorescence quenching by charges was studied previously in a range of fluorescent materials using steady-state photoluminescence (PL) measurements in electrochemically doped films.<sup>10,14,15</sup> These measurements can quantify the magnitude of quenching but they give very limited information on the quenching mechanism and the role of exciton diffusion in fluorescence quenching. In the present work we use time-resolved PL measurements to study PFO films containing the  $\beta$ -phase as they are

1  
2  
3 electrochemically doped over a wide range of charge concentrations. This allows us to  
4  
5 understand the quenching mechanism and its effect on device performance.  
6  
7

8 The structure of this paper is as follows. First we demonstrate electrochemical doping of  
9  
10 PFO films and show its effect on fluorescence decays for low, high and intermediate charge  
11  
12 densities. Then the data are analyzed using simple kinetic models and the rate constants for  
13  
14 quenching are extracted. Finally, the dependence of the OLED efficiency on current density is  
15  
16 modelled using the obtained parameters and published data.  
17  
18  
19  
20  
21

## 22 **2. EXPERIMENTAL METHODS**

23  
24

25 Poly[9,9-dioctylfluorenyl-2,7-diyl] (PFO) was purchased from American Dye Source  
26  
27 (product ADS129BE). Polymer films were spin-coated from solutions in tetrahydrofuran  
28  
29 (Sigma-Aldrich) over indium-tin oxide (ITO) covered glass substrates (Delta,  $R_s = 15\text{-}25 \Omega/\square$ )  
30  
31 which were cleaned by sonication in an acetone bath prior to spin-coating. Film thickness  
32  
33 were determined by Dektak surface profiler.  
34  
35

36  
37 *In situ* spectroelectrochemical measurements (absorption, steady state and time-  
38  
39 resolved PL) were performed in a modified 1 cm length fused silica cell capped with a Teflon  
40  
41 plate which also served as electrode support.<sup>15</sup> ITO covered with the polymer was used as a  
42  
43 working electrode immersed in a solution of 0.1 M tetrabutylammonium tetrafluoroborate  
44  
45 (Sigma-Aldrich, electrochemical grade) in anhydrous acetonitrile (Sigma-Aldrich). The  
46  
47 counter electrode was a platinum wire and a silver wire was used as the pseudo-reference  
48  
49 electrode both immersed in the same solution and protected by a glass capillary tube. The  
50  
51 electrochemical measurements were performed with a Dropsens  $\mu$ Stat400 potentiostat-  
52  
53 galvanostat. The potential of the reference electrode was calibrated versus ferrocene (Fc),  
54  
55 added to the cell at the end of the experiments. The electrochemical potentials are expressed  
56  
57  
58  
59  
60

1  
2  
3 with respect to that reference. The time-resolved PL was spectrally integrated in the range  
4 430-520 nm and measured with ~2 ps time resolution using a Hamamatsu C6860 streak  
5 camera in synchroscan mode following excitation by 100 fs pulses at 400 nm and 80 MHz  
6 produced by a frequency doubled mode-locked Ti:sapphire laser. The excitation density was  
7 kept low, below  $10^{14}$  cm<sup>-3</sup>, to avoid exciton-exciton interactions.  
8  
9  
10  
11  
12

### 13 14 **3. RESULTS**

15  
16  
17 The films of PFO were spin-coated on indium-tin oxide (ITO) covered glass substrate  
18 and immersed in the electrochemical cell containing acetonitrile and supporting electrolyte.  
19 The cyclic voltammogram is shown in Figure 1A and indicates that oxidation onset of the  
20 conjugated polymer chains occurs at the 0.53 V potential versus ferrocene (Fc).  
21  
22  
23  
24  
25  
26

27 The hole density in the polymer film was determined by integrating the oxidation  
28 current in the forward scan of the stabilized voltammogram and is shown in Figure 1B as a  
29 function of the applied electrochemical potential. The error in the hole density is mainly  
30 determined by the current range in the potentiostat and is on the order of  $10^{14}$  cm<sup>-3</sup>. Figure 1C  
31 shows the absorption and photoluminescence (PL) spectra of PFO film used in this study. The  
32 absorption peak at 437 nm corresponds to the 0-0 vibronic transition in  $\beta$ -phase PFO whereas  
33 the absorption of the  $\beta$ -phase and glassy phase overlap at <420 nm. The fraction of PFO  
34 chromophores which adopt  $\beta$ -phase configuration was determined to be 33% by subtracting  
35 the glassy phase absorbance.<sup>16,17</sup> The PL spectra of the PFO films show peaks at 441, 468, and  
36 500 nm which correspond well to the vibronic progression of  $\beta$ -phase photoluminescence. No  
37 fluorescence of glassy phase is observed suggesting fast energy transfer from glassy to  $\beta$   
38 phase. This indicates that both phases are intimately mixed in these films. Figure 1D shows  
39 electrochemically induced absorption spectra in a PFO film at three different doping levels.  
40 The main absorption peak at 642 nm and shoulders at around 590 nm and 540 nm are  
41  
42  
43  
44  
45  
46  
47  
48  
49  
50  
51  
52  
53  
54  
55  
56  
57  
58  
59  
60

1  
2  
3 characteristic of hole polarons residing in the  $\beta$  phase of PFO films.<sup>16</sup> The main peak shows a  
4 linear increase with hole density up to of  $2 \times 10^{19} \text{ cm}^{-3}$  and this allows us to determine the  
5 absorption cross-section of  $4 \times 10^{16} \text{ cm}^2$  for hole polarons at 642 nm which is consistent with  
6 literature values.<sup>16,18</sup> This gives us independent verification of the charge densities in our  
7 experiments.  
8  
9  
10  
11  
12

13  
14 Figure 2 shows the photoluminescence (PL) kinetics measured at different hole  
15 densities. As the hole density increases, the PL decays get faster which indicates dynamical  
16 fluorescence quenching by electrochemically injected holes. The results are reproducible up  
17 to a doping level of  $2 \times 10^{20} \text{ cm}^{-3}$  and indicate that no sample degradation occurs at these  
18 conditions. Moving the laser excitation spot onto different positions of the sample also gave  
19 reproducible results.  
20  
21  
22  
23  
24  
25  
26

27  
28 The PL lifetime in undoped PFO film is 142 ps and similar to the previously found  
29 170 ps PL lifetime in films with a high proportion of  $\beta$ -phase.<sup>17</sup> The PL lifetime decreases by  
30 a factor of two when the hole density increases to  $2 \times 10^{18} \text{ cm}^{-3}$  and by a factor of five for a  
31 hole density of  $10^{19} \text{ cm}^{-3}$  (Figure 2B). The observed decrease of PL lifetime is qualitatively  
32 similar to polymer-fullerene blends where a complete quenching of polymer fluorescence is  
33 generally observed for fullerene concentrations of  $5 \times 10^{19}$  sites per  $\text{cm}^3$ .<sup>19</sup> Such charge  
34 densities can easily be reached in light-emitting field-effect transistors and in doped regions of  
35 electrochemical cells. Understanding the mechanism of quenching can help to develop  
36 strategies to improve the efficiency of devices.  
37  
38  
39  
40  
41  
42  
43  
44  
45  
46  
47

48  
49 The time-resolved PL intensity is proportional to the density of singlet excitons which  
50 in undoped polymer ( $n_{undoped}$ ) decays in time with rate constant  $k$  according to  
51  
52

$$\frac{dn_{undoped}}{dt} = -kn_{undoped} \quad (1)$$

Here we assumed an instantaneous generation of excitons which is the case in our experiment with 200 fs excitation pulses. In doped polymer films there is an additional decay path that occurs when a singlet exciton ( $S_1^*$ ) encounters a hole polaron ( $p^+$ ):  $S_1^* + p^+ \rightarrow S_0 + p^+ + \text{phonons}$ . Hence the exciton density in doped polymer  $n_{doped}$  evolves following

$$\frac{dn_{doped}}{dt} = -kn_{doped} - k_q n_{doped} \quad (2)$$

where  $k_q$  is the quenching rate due to the electrochemical doping. Combining Equation (1) and (2), we get

$$k_q = -\frac{d}{dt} \ln[g(t)] \quad (3)$$

where  $g(t) = \frac{n_{doped}}{n_{undoped}}$  is the ratio of the PL intensity in the doped film to that of the undoped film.

We begin by considering the limiting cases of low and high doping. **Figure 3** shows the time dependence of the natural logarithm of the PL ratio  $g(t)$  at low doping levels. It is approximately linear and indicates that fluorescence quenching can be described by a time-independent  $k_q$  which is obtained from the slope of linear fits according to Equation (3).

The time-independent  $k_q$  indicates that uniform distribution of emitters and quenchers is maintained in the film over the PL lifetime by fast exciton diffusion. From the linear fit to the  $k_q$  dependence on the hole density  $N$  we obtain the rate constant of singlet exciton quenching per injected polaron  $\gamma_{sp} = \frac{k_q}{N} = (2.4 \pm 0.4) \times 10^{-9} \text{ cm}^3 \text{ s}^{-1}$  (Figure 3B). This value is twice higher than reported in the ladder-type polymer m-LPPP which shows absorption and fluorescence spectra similar to PFO with  $\beta$  phase.<sup>20</sup> It is interesting that  $\gamma_{sp}$  is about eight times lower than the rate constant for singlet-singlet exciton annihilation of  $2 \times 10^{-8} \text{ cm}^3 \text{ s}^{-1}$  reported

1  
2  
3 in PFO films with a similar amount of  $\beta$  phase.<sup>21,22</sup> The reasons for this are explained in the  
4  
5 discussion section.

6  
7  
8 . In the limiting case of high doping a direct Förster resonance energy transfer (FRET)  
9  
10 to holes is expected to dominate quenching. For FRET-only quenching in the point-dipole  
11  
12 approximation the dynamics of PL ratio  $g(t)$  would follow:<sup>23</sup>  
13

$$14 \quad g(t) = g_0 \exp(-\beta t^{1/2}) \quad (4)$$

$$15 \quad \text{where} \quad \beta = \frac{4}{3} \pi^{3/2} R_0^3 N \tau^{-0.5} \quad (5)$$

16  
17  
18 Here  $R_0$  is the Förster radius for FRET and  $\tau$  is the fluorescence lifetime of the  
19  
20 undoped polymer. Then, according to Equation (4), the natural logarithm of PL ratio should  
21  
22 be linear with respect the square root of time which is observed in highly doped polymer  
23  
24 (Figure 4). From the linear fits and Equation (5) with  $\tau=142$  ps we obtain  $R_0=2.5$  nm for  
25  
26 charge densities in a range of  $(1.7-5.5) \times 10^{18} \text{ cm}^{-3}$  and  $R_0=2.4$  nm for  $1.0 \times 10^{19} \text{ cm}^{-3}$ .  
27  
28  
29  
30  
31  
32  
33

34 The kinetics of PL quenching at intermediate doping levels are shown in Figure 5. The  
35  
36 decay of  $\ln[g(t)]$  is no longer a straight line which indicates that quenching rate is time  
37  
38 dependent. Because quenching at high doping occurs by FRET, it is reasonable to assume that  
39  
40 diffusion and FRET both would contribute to quenching at intermediate doping. In that case  
41  
42 the PL ratio  $g(t)$  can be fitted with the following equation:<sup>23</sup>  
43  
44

$$45 \quad g(t) = g_0 \exp(-\alpha t - \beta t^{1/2}) \quad (6)$$

46  
47  
48 where  $\alpha$  is a time-independent decay rate constant which describes diffusion-assisted  
49  
50 quenching and  $\beta$  is a coefficient which describes the direct FRET. We have previously applied  
51  
52 this approach to describe the fluorescence quenching in other conjugated polymer films by  
53  
54 dispersed fullerene molecules.<sup>19</sup> The solid lines in Figure 5 show the fits to Equation (6) and  
55  
56  
57

the values of  $\alpha$  and  $\beta$  coefficients obtained from the fits are presented in Figure 6. The time-independent rate,  $\alpha$ , and the time-dependent rate,  $\beta$ , both grow approximately linearly with hole density up to a doping level of  $4 \times 10^{18} \text{ cm}^{-3}$ .

The migration-limited quenching rate constant can be obtained from the linear dependence of  $\alpha$  on hole density using  $\gamma_{sp} = \frac{\alpha}{N}$  and gives  $(1.7 \pm 0.2) \times 10^{-9} \text{ cm}^3 \text{ s}^{-1}$ . This value has to be considered a lower bound because in our analysis we attributed the time-dependent rate solely to FRET whilst in fact a fraction of the time-dependent component may occur because of dispersive exciton diffusion. On other hand, the value  $\gamma_{sp} = \frac{k_q}{N} = (2.4 \pm 0.4) \times 10^{-9} \text{ cm}^3 \text{ s}^{-1}$  obtained at low charge density represents an upper bound because contribution of direct FRET was not accounted for. We take an average of these two limiting values and get  $\gamma_{sp} = (2.0 \pm 0.3) \times 10^{-9} \text{ cm}^3 \text{ s}^{-1}$ . From the linear fit in Figure 6B we get  $R_0 = 2.7 \pm 0.2 \text{ nm}$  which is slightly higher than the values obtained at very high charge densities. Previously we reported a slight saturation of hole polaron absorption at high doping levels and a blue shift which we attributed to compressed polarons because of Coulombic repulsion between them in highly doped samples.<sup>16</sup> Lower absorption cross-section of the compressed polaron can explain lower values of the Förster radius at high doping levels and at least in part the saturation of quenching rate constants when hole density exceeds  $6 \times 10^{18} \text{ cm}^{-3}$ .

In these experiments the fraction of fluorescence quenching produced by direct FRET to polaron  $f_{FRET}$  can be estimated using

$$f_{FRET} = \frac{\int_0^{\infty} [\exp(-\alpha t) - \exp(-\alpha t - \beta t^{1/2})] dt}{\int_0^{\infty} \exp(-\alpha t) dt} \quad (7)$$

The results for  $N$  up to  $10^{19} \text{ cm}^{-3}$  are shown in Figure 7. The FRET contribution to quenching is below 20% at hole density below  $1 \times 10^{17} \text{ cm}^{-3}$  and increases when more holes are injected.

1  
2  
3 The  $f_{FRET}=0.5$  point indicates the charge density at which the contributions of quenching from  
4 direct FRET and from diffusion-assisted process are equal. This occurs at charge density of  
5 about  $5 \times 10^{18} \text{ cm}^{-3}$  for PFO films. At hole densities below  $10^{18} \text{ cm}^{-3}$  quenching is assisted by  
6 exciton diffusion and can be reduced by diluting the emitting chromophores. At higher charge  
7 densities, the direct FRET to polarons is significant and in order to reduce it one should  
8 decrease the spectral overlap of luminescence with polaron absorption or spatially separate  
9 the light-emission zone from the charge recombination zone.  
10  
11  
12  
13  
14  
15  
16  
17  
18  
19  
20

#### 21 4. DISCUSSION

22  
23 Our results indicate homogeneous charge distribution within the film at all doping levels. The  
24 evidence comes from the time-independent rate constant of quenching observed at low charge  
25 density (Figure 3). If the doping was a surface phenomenon, then the quenching rate would be  
26 time-dependent because the excitons generated further from the surface would be quenched  
27 slower than the excitons near the surface. At high doping level we observe very fast  
28 quenching which can be described as a single step Förster-type energy transfer (Figure 4). If  
29 charges were piling at the surface, then we would observe a longer lived fluorescence  
30 component from excitons generated further away from film surface.  
31  
32  
33  
34  
35  
36  
37  
38  
39

40 Now we discuss possible reasons why the rate constant for fluorescence quenching by  
41 polarons in the diffusion-assisted regime is an order of magnitude smaller than the singlet-  
42 singlet exciton annihilation constant. If quenching occurs on a first encounter with a hole and  
43 is faster than diffusion, then the quenching rate constant is diffusion-limited and in the long  
44 time limit can be described by the solution of the Smoluchowski equation  
45  
46  
47  
48  
49  
50

$$51 \gamma_{sp} = 4\pi(D_s + D_h)R_{sp} \quad (8)$$

52  
53  
54  
55  
56  
57

where  $D_s$  and  $D_h$  are diffusivities of singlet exciton and hole, and  $R_{sp}$  is an effective annihilation radius for singlet exciton and hole polaron. When quenching occurs by FRET and can be described by a point dipole approximation, the following estimate can be used<sup>23</sup>

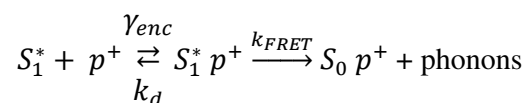
$$R_{sp} = 0.676 \left( \frac{R_0^6}{\tau D_s} \right)^{1/4} \quad (9)$$

where  $\tau$  is the fluorescence lifetime. Then using  $R_0=2.7$  nm and  $\tau=142$  ps from this work and  $D_s=0.012$  cm<sup>2</sup>s<sup>-1</sup> reported in PFO films<sup>21,22,24</sup> we get  $R_{sp}\approx 0.8$  nm. Similarly, one exciton is lost per singlet-singlet annihilation event, hence

$$\gamma_{ss} = 4\pi D_s R_{ss} \quad (10)$$

where  $R_{ss}$  is an effective singlet-singlet exciton annihilation radius. Using the reported hole mobility  $\mu_h=5\times 10^{-5}$  cm<sup>2</sup> V<sup>-1</sup>s<sup>-1</sup> in PFO with 1.3% of  $\beta$  phase<sup>7</sup> and the Einstein relation  $D=\mu k_B T/e$  we estimate the hole diffusivity  $D_h \approx 1.2\times 10^{-6}$  cm<sup>2</sup>s<sup>-1</sup>  $\ll D_s$ . Then the findings  $\gamma_{ss} \approx 10\gamma_{sp}$  and  $R_{sp}\approx 0.8$  nm would imply  $R_{ss}\approx 8$  nm if both quenching processes were diffusion-limited. Singlet-singlet annihilation occurs by FRET onto excited chromophore, thus from Equation (9) we get  $R_{ss} = a(R_e/R_g)^{3/2}$ , where  $a$  is the inter-chromophore distance whilst  $R_e$  and  $R_g$  are the Förster radii for energy transfer to the chromophore in excited and ground state, respectively. Using  $a=1.28$  nm which is the inter-chain distance of aligned PFO chains determined by grazing incidence X-ray diffraction<sup>25</sup> we get  $R_e\approx 3.4R_g$  which would require strong overlap of emission and excited state absorption spectra. However, this would be incompatible with high optical gain observed in PFO films over the whole emission band.<sup>26</sup> We therefore consider it more likely that polarons are not perfect quenchers for singlet excitons and exciton can escape FRET to polaron by diffusing away. This can happen because the estimated  $R_{sp}\approx 0.8$  nm is substantially shorter than an average inter-chain distance between PFO chains  $a=1.28$  nm. Singlet excitons simply cannot get close enough to the holes to be

irreversibly quenched by FRET. The interaction with a non-perfect quencher can be analysed using Scheme 1.



**Scheme 1.** Quenching of singlet exciton  $S_1^*$  by FRET to hole polaron  $p^+$ .

Here  $\gamma_{enc}$  is a second order rate constant which describes exciton diffusion to a polaron to form an encounter complex  $S_1^* p^+$  whilst  $k_d$  and  $k_{FRET}$  are first order rate constants which describe the escape of exciton from polaron and FRET to a polaron, respectively. Then the overall exciton quenching rate constant can be expressed as

$$\gamma_{sp} = \frac{\gamma_{enc} k_{FRET}}{k_d + k_{FRET}} \quad (11)$$

In the limiting case when  $k_{FRET} \gg k_d$ , then  $\gamma_{sp} \approx \gamma_{enc}$  and quenching is migration-limited. We can estimate  $k_d$  from the singlet exciton diffusivity  $D_s$  in PFO by a random walk

$$k_d = \frac{z D_s}{a^2} \quad (12)$$

where  $z$  is the number of the nearest neighbors and  $a$  is the distance to these nearest neighbors. Energy transfer in the direction of side chains is expected to be slow because of large inter-chromophore spacing, hence, we assume  $z=4$ . Then using  $D_s = 0.012 \text{ cm}^2 \text{ s}^{-1}$  and  $a = 1.28 \text{ nm}$  as an average inter-chain distance we get  $k_d = 2.9 \text{ ps}^{-1}$ .

An upper limit for  $k_{FRET}$  can be estimated using the point-dipole approximation

$$k_{FRET} = \tau^{-1} \left( \frac{R_0}{a} \right)^6 \quad (13)$$

where  $\tau$  is the fluorescence lifetime of the pristine PFO. Using  $R_0 = 2.7 \text{ nm}$  and  $a = 1.28 \text{ nm}$  we get  $k_{FRET} \approx 0.6 \text{ ps}^{-1}$ . This is an upper limit because point-dipole approximation is known to overestimate  $k_{FRET}$  between conjugated polymer chromophores at short distances.<sup>27</sup> Using these values in Equation (11) gives  $\gamma_{sp} < 0.17 \gamma_{enc}$  which is consistent with our experimental finding  $\gamma_{sp} \approx 0.1 \gamma_{ss}$ .

Next we assess the impact of exciton-polaron interactions on OLED efficiency. For simplicity we assume that the hole (and electron) density  $N$  is constant over a thickness  $d$  of the electron-hole recombination zone and that all injected charges recombine. Then the number of injected carriers per unit time and area is equal to the number of carriers recombined, hence

$$\frac{j}{e} = \gamma_{eh} N^2 d \quad (13)$$

where  $j$  is the current density,  $e$  is elementary charge and  $\gamma_{eh}$  is the electron-hole recombination rate constant. Assuming that recombination occurs on the first encounter, it can be described by Langevin equation

$$\gamma_{eh} = \frac{e(\mu_e + \mu_h)}{\epsilon_0 \epsilon} \quad (14)$$

where  $\mu_e$  and  $\mu_h$  are electron and hole mobility, respectively, whilst  $\epsilon_0$  and  $\epsilon$  are vacuum and relative permittivity. Combining (13) and (14) we get

$$N = \frac{1}{e} \sqrt{\frac{j \epsilon_0 \epsilon}{(\mu_e + \mu_h) d}} \quad (15)$$

Assuming that 25% of recombining electron-hole pairs form singlet excitons and the remaining 75% form triplet excitons, the steady state density of singlet excitons  $n_S$  and of triplet excitons  $n_T$  can be estimated using

$$n_S = \frac{j \tau_S}{4ed} \quad \text{and} \quad n_T = \frac{3j \tau_T}{4ed} \quad (16)$$

where  $\tau_S$  and  $\tau_T$  are lifetimes of singlet and triplet exciton, respectively. Figure 8 shows the average density of electrons and holes ( $2N$ ) calculated using Equation (15) and the density of singlet and triplet excitons estimated using Equation (16).

We assumed  $\epsilon=3$  and  $d=100$  nm which is a typical thickness of the light emitting layer in OLEDs. We used the lower bound of the reported hole mobility values in PFO with  $\beta$ -phase  $\mu_h=4\times 10^{-6}$  cm<sup>2</sup> V<sup>-1</sup>s<sup>-1</sup> to get an upper estimate of the polaron density.<sup>28</sup> We assumed  $\mu_e=\mu_h$  and used  $\tau_S=250$  ps found in PFO films with a small amount of  $\beta$ -phase<sup>17</sup>. For triplet lifetime we used a value  $\tau_T=108$   $\mu$ s reported for PFO in solution.<sup>29</sup> For this long triplet exciton lifetime the triplet density is higher than the density of electrons and holes. In these calculations we have neglected triplet-triplet exciton annihilation which can occur at high triplet exciton densities but is unlikely to have significant effect in PFO with diluted  $\beta$  phase because this phase acts as an effective trap for triplet excitons.<sup>30</sup>

Assuming that hole and electron polarons quench singlet excitons with the same rate constant  $\gamma_{sp}$  the dynamics of singlet excitons in an OLED can be described by the rate equation

$$\frac{dn_S}{dt} = \gamma_{eh}N^2 - \frac{n_S}{\tau_S} - 2\gamma_{sp}n_SN - \gamma_{ss}n_S^2 - \gamma_{st}n_Sn_T \quad (17)$$

where  $\gamma_{st}$  is the singlet-triplet annihilation rate constant. The internal quantum efficiency (IQE) of fluorescent OLED is proportional to the singlet exciton density  $n_S$  under steady state conditions, so, the IQE roll-off because of fluorescence quenching by electrons and holes can be estimated using

$$\frac{IQE}{IQE_{max}} = (1 + 2\gamma_{sp}N\tau_S)^{-1} \quad (18)$$

The effect of singlet-singlet and singlet-triplet annihilation can be estimated using

$$\frac{IQE}{IQE_{max}} = (1 + \gamma_{ss}n_S\tau_S)^{-1} \quad \text{and} \quad \frac{IQE}{IQE_{max}} = (1 + \gamma_{st}n_T\tau_S)^{-1} \quad (19)$$

Figure 8 shows the calculated efficiency roll-off using  $\gamma_{sp}=2\times 10^{-9}$  cm<sup>3</sup>s<sup>-1</sup> from this work and  $\gamma_{ss}=2\times 10^{-8}$  cm<sup>3</sup>s<sup>-1</sup> found in PFO with 20-30% of  $\beta$ -phase.<sup>21</sup> To estimate  $\gamma_{st}$  we used

Equation (11) and the Förster radius for FRET to triplet exciton  $R_0=2.1$  nm which was calculated using the spectral overlap of fluorescence and triplet absorption in polyfluorene.<sup>24</sup>

In the point dipole approximation using Equation (13) and Förster radii for FRET to triplet and to polaron we get  $\gamma_{st} \approx 0.2\gamma_{sp} = 4 \times 10^{-10} \text{ cm}^3 \text{ s}^{-1}$ . The low  $\gamma_{st}$  value is consistent with the experiments which found that triplets generated in polyfluorene films with continuous excitation of  $100 \text{ mWcm}^{-2}$  had negligible effect on singlet exciton dynamics.<sup>24</sup> The simulated results in Figure 8 predict that singlet-triplet annihilation is the main mechanism limiting OLED efficiency at high current and the simulated efficiency roll-off is very similar to the experimentally observed roll-off (symbols in Figure 8) without any adjustment of the parameters. The simulations suggest that fluorescence quenching by charges is a second major mechanism for the efficiency roll-off at high current densities whilst singlet-singlet annihilation has negligible effect even at very high current. We also calculated the efficiency roll-off by singlet-triplet annihilation for a shorter triplet lifetime  $\tau_T = 1 \text{ } \mu\text{s}$  and found it to be significant only at current densities exceeding  $0.1 \text{ A/cm}^2$ . This suggests that device efficiency at high brightness could be significantly improved using triplet quenchers. Of course, these would need to be selected so as not to quench singlets – an issue that has been explored in the context of organic semiconductor lasers.<sup>31,32</sup> In that case fluorescence quenching by charges would be the main efficiency roll-off mechanism at high current densities.

## 5. CONCLUSIONS

We studied quenching of excitons by charges in the blue electroluminescent polymer PFO. We observed two fluorescence quenching mechanisms upon charge injection: exciton diffusion assisted quenching at low charge densities and direct Förster resonance energy transfer (FRET) which dominates at charge densities above  $5 \times 10^{18} \text{ cm}^{-3}$ . The Förster radius

1  
2  
3 for resonance energy transfer to holes is found to be  $2.7\pm 0.2$  nm whilst the diffusion-assisted  
4 quenching rate constant is  $2\times 10^{-9}$  cm<sup>3</sup> s<sup>-1</sup>. The diffusion-mediated quenching rate constant is  
5 ten times lower than the reported rate constant for singlet-singlet annihilation and indicates  
6 that only one in ten exciton-hole encounters leads to quenching whilst in the remainder the  
7 exciton can diffuse away avoiding quenching. We estimate that fluorescence quenching by  
8 charges is the second major mechanism for the efficiency roll-off at high current densities in  
9 light-emitting diodes using PFO with  $\beta$  phase after singlet-triplet exciton annihilation. Our  
10 results suggest that if the OLED efficiency using PFO at high brightness can be improved  
11 using triplet quenchers, then fluorescence quenching by charges can become the main  
12 efficiency roll-off mechanism at high current densities. These results are important for high  
13 brightness organic optoelectronic devices such as OLEDs for outdoor displays, lighting,  
14 optogenetics and the development of electrically pumped lasers. They help understand why,  
15 very high efficiencies can be achieved in OLEDs, even though the devices are full of polarons,  
16 and polarons are known to quench luminescence.  
17  
18  
19  
20  
21  
22  
23  
24  
25  
26  
27  
28  
29  
30  
31  
32  
33  
34  
35  
36

### 37 ACKNOWLEDGEMENTS

38  
39  
40 The authors acknowledge financial support from the European Research Council  
41 (grant 321305), Spanish Ministry of Economy *Explora Ciencia* Project MAT2013-49534-  
42 EXP and the Engineering and Physical Sciences Research Council (grants EP/L017008/1 and  
43 EP/J009016/1). I.D.W.S. also acknowledges support from a Royal Society Wolfson Research  
44 Merit Award. The research data supporting this publication can be accessed at DOI:  
45 <http://dx.doi.org/10.17630/70a7c842-48a0-498b-9d7e-e18b3f9b372c>  
46  
47  
48  
49  
50  
51  
52  
53  
54  
55  
56  
57  
58  
59  
60

**REFERENCES**

- (1) Gather, M. C.; Köhnen, A.; Meerholz, K. White Organic Light-Emitting Diodes. *Adv. Mater.* **2011**, *23*, 233–248.
- (2) Reineke, S.; Lindner, F.; Schwartz, G.; Seidler, N.; Walzer, K.; Lüssem, B.; Leo, K. White Organic Light-Emitting Diodes with Fluorescent Tube Efficiency. *MRS Proc.* **2009**, *1212*, 1212-S02-6.
- (3) Reineke, S.; Thomschke, M.; Lüssem, B.; Leo, K. White Organic Light-Emitting Diodes: Status and Perspective. *Rev. Mod. Phys.* **2013**, *85*, 1245–1293.
- (4) Zhongbin, W.; Dongge, M. Recent Advances in White Organic Light-Emitting Diodes. *Mater. Sci. Eng. R Reports* **2016**, *107*, 1–42.
- (5) Scholz, S.; Kondakov, D.; Lüssem, B.; Leo, K. Degradation Mechanisms and Reactions in Organic Light-Emitting Devices. *Chem. Rev.* **2015**, *115*, 8449–8503.
- (6) Giebink, N. C.; Forrest, S. R. Quantum Efficiency Roll-Off at High Brightness in Fluorescent and Phosphorescent Organic Light Emitting Diodes. *Phys. Rev. B* **2008**, *77*, 235215.
- (7) Lu, H.-H.; Liu, C.-Y.; Chang, C.-H.; Chen, S.-A. Self-Dopant Formation in Poly(9,9-Di-N-Octylfluorene) Via a Dipping Method for Efficient and Stable Pure-Blue Electroluminescence. *Adv. Mater.* **2007**, *19*, 2574–2579.
- (8) Zhang, X.; Hu, Q.; Lin, J.; Lei, Z.; Guo, X.; Xie, L.; Lai, W.; Huang, W. Efficient and Stable Deep Blue Polymer Light-Emitting Devices Based on  $\beta$ -Phase poly(9,9-Di-octylfluorene). *Appl. Phys. Lett.* **2013**, *103*, 153301.
- (9) Zhang, Q.; Chi, L.; Hai, G.; Fang, Y.; Li, X.; Xia, R.; Huang, W.; Gu, E. An Easy

- 1  
2  
3 Approach to Control  $\beta$ -Phase Formation in PFO Films for Optimized Emission  
4  
5 Properties. *Molecules* **2017**, *22*, 315.  
6  
7
- 8 (10) van Reenen, S.; Vitorino, M. V; Meskers, S. C. J.; Janssen, R. A. J.; Kemerink, M.  
9  
10 Photoluminescence Quenching in Films of Conjugated Polymers by Electrochemical  
11  
12 Doping. *Phys. Rev. B* **2014**, *89*, 205206.  
13  
14
- 15 (11) Montilla, F.; Frutos, L. M.; Mateo, C. R.; Mallavia, R. Fluorescence Emission  
16  
17 Anisotropy Coupled to an Electrochemical System: Study of Exciton Dynamics in  
18  
19 Conjugated Polymers. *J. Phys. Chem. C* **2007**, *119*, 18405–18410.  
20  
21  
22
- 23 (12) Palacios, R. E.; Chang, W. S.; Grey, J. K.; Chang, Y. L.; Miller, W. L.; Lu, C. Y.;  
24  
25 Henkelman, G.; Zepeda, D.; Ferraris, J.; Barbara, P. F. Detailed Single-Molecule  
26  
27 Spectroelectrochemical Studies of the Oxidation of Conjugated Polymers. *J. Phys.*  
28  
29 *Chem. B* **2009**, *113*, 14619–14628.  
30  
31
- 32 (13) Bolinger, J. C.; Traub, M. C.; Adachi, T.; Barbara, P. F. Ultralong-Range Polaron-  
33  
34 Induced Quenching of Excitons in Isolated Conjugated Polymers. *Science*. **2011**, *331*,  
35  
36 565–567.  
37  
38
- 39 (14) Montilla, F.; Mallavia, R. In Situ Electrochemical Fluorescence Studies of PPV. *J.*  
40  
41 *Phys. Chem. B* **2006**, *110*, 25791–25796.  
42  
43  
44
- 45 (15) Montilla, F.; Pastor, I.; Mateo, C. R.; Morallon, E.; Mallavia, R.; Morallón, E.;  
46  
47 Mallavia, R. Charge Transport in Luminescent Polymers Studied by in Situ  
48  
49 Fluorescence Spectroscopy. *J. Phys. Chem. B* **2006**, *110*, 5914–5919.  
50  
51
- 52 (16) Montilla, F.; Ruseckas, A.; Samuel, I. D. W. Absorption Cross-Sections of Hole  
53  
54 Polarons in Glassy and Beta-Phase Polyfluorene. *Chem. Phys. Lett.* **2013**, *585*, 133–  
55  
56 137.  
57

- 1  
2  
3 (17) Bansal, A. K.; Ruseckas, A.; Shaw, P. E.; Samuel, I. D. W. Fluorescence Quenchers in  
4 Mixed Phase Polyfluorene Films. *J. Phys. Chem. C* **2010**, *114*, 17864–17867.  
5  
6  
7  
8 (18) Montilla, F.; Huerta, F. Electrochemically Monitored Photoluminescence of  
9 Conjugated Polymers. In *Luminescence in Electrochemistry*; Springer International  
10 Publishing: Cham, 2017; pp 105–137.  
11  
12  
13  
14  
15 (19) Ward, A. J.; Ruseckas, A.; Samuel, I. D. W. A Shift from Diffusion Assisted to Energy  
16 Transfer Controlled Fluorescence Quenching in Polymer-Fullerene Photovoltaic  
17 Blends. *J. Phys. Chem. C* **2012**, *116*, 23931–23937.  
18  
19  
20  
21  
22 (20) List, E. J. W.; Kim, C. H.; Naik, A. K.; Scherf, U.; Leising, G.; Graupner, W.; Shinar, J.  
23 Interaction of Singlet Excitons with Polarons in Wide Band-Gap Organic  
24 Semiconductors: A Quantitative Study. *Phys. Rev. B* **2001**, *64*, 155204.  
25  
26  
27  
28  
29  
30 (21) Shaw, P. E.; Ruseckas, A.; Peet, J.; Bazan, G. C.; Samuel, I. D. W. Exciton-Exciton  
31 Annihilation in Mixed-Phase Polyfluorene Films. *Adv. Funct. Mater.* **2010**, *20*, 155–  
32 161.  
33  
34  
35  
36  
37 (22) Stevens, M. A.; Silva, C.; Russell, D. M.; Friend, R. H. Exciton Dissociation  
38 Mechanisms in the Polymeric Semiconductors poly(9,9-Dioctylfluorene) and poly(9, 9-  
39 Dioctylfluorene-Co-Benzothiadiazole). *Phys. Rev. B* **2001**, *63*, 165213 .  
40  
41  
42  
43  
44  
45 (23) Gosele, U.; Hauser, M.; Klein, U. K. A.; Frey, R. Diffusion and Long-Range Energy-  
46 Transfer. *Chem. Phys. Lett.* **1975**, *34*, 519–522.  
47  
48  
49  
50 (24) King, S. M.; Dai, D.; Rothe, C.; Monkman, A. P. Exciton Annihilation in a  
51 Polyfluorene: Low Threshold for Singlet-Singlet Annihilation and the Absence of  
52 Singlet-Triplet Annihilation. *Phys. Rev. B* **2007**, *76*, 085204  
53  
54  
55  
56  
57

- 1  
2  
3 (25) Kawana, S.; Durrell, M.; Lu, J.; Macdonald, J. E.; Grell, M.; Bradley, D. D. C.; Jukes,  
4 P. C.; Jones, R. A. L.; Bennett, S. L. X-Ray Diffraction Study of the Structure of Thin  
5 Polyfluorene Films. *Polymer*. **2002**, *43*, 1907–1913.  
6  
7  
8  
9  
10 (26) Marciniak, H.; Teicher, M.; Scherf, U.; Trost, S.; Riedl, T.; Lehnhardt, M.; Rabe, T.;  
11 Kowalsky, W.; Lochbrunner, S. Photoexcitation Dynamics in Polyfluorene-Based Thin  
12 Films: Energy Transfer and Amplified Spontaneous Emission. *Phys. Rev. B* **2012**, *85*,  
13 214204.  
14  
15  
16  
17  
18  
19 (27) Shaw, P. E.; Ruseckas, A.; Samuel, I. D. W. Distance Dependence of Excitation  
20 Energy Transfer between Spacer-Separated Conjugated Polymer Films. *Phys. Rev. B*  
21 **2008**, *78*, 245201  
22  
23  
24  
25  
26 (28) Bai, Z.; Liu, Y.; Li, T.; Li, X.; Liu, B.; Liu, B.; Lu, D. Quantitative Study on  $\beta$ -Phase  
27 Heredity Based on Poly(9,9-Dioctylfluorene) from Solutions to Films and the Effect on  
28 Hole Mobility. *J. Phys. Chem. C* **2016**, *120*, 27820–27828.  
29  
30  
31  
32  
33 (29) Burrows, H. D.; Seixas de Melo, J.; Serpac, C.; Arnaut, L.; Miguel, M.; Monkman, A.  
34 P.; Hamblet, I.; Navaratnam, S. Triplet State Dynamics on Isolated Conjugated  
35 Polymer Chains. *Chem. Phys.* **2002**, *285*, 3–11.  
36  
37  
38  
39  
40 (30) Rothe, C.; King, S.; Dias, F.; Monkman, A. Triplet Exciton State and Related  
41 Phenomena in the  $\beta$ -Phase of poly(9,9-Dioctyl)fluorene. *Phys. Rev. B* **2004**, *70*, 195213.  
42  
43  
44  
45  
46 (31) Gärtner, C.; Karnutsch, C.; Lemmer, U.; Pflumm, C. The Influence of Annihilation  
47 Processes on the Threshold Current Density of Organic Laser Diodes. *J. Appl. Phys.*  
48 **2007**, *101*, 23107.  
49  
50  
51  
52  
53 (32) Zhang, Y.; Forrest, S. R. Existence of Continuous-Wave Threshold for Organic  
54 Semiconductor Lasers. *Phys. Rev. B* **2011**, *84*, 241301.  
55  
56  
57  
58  
59  
60

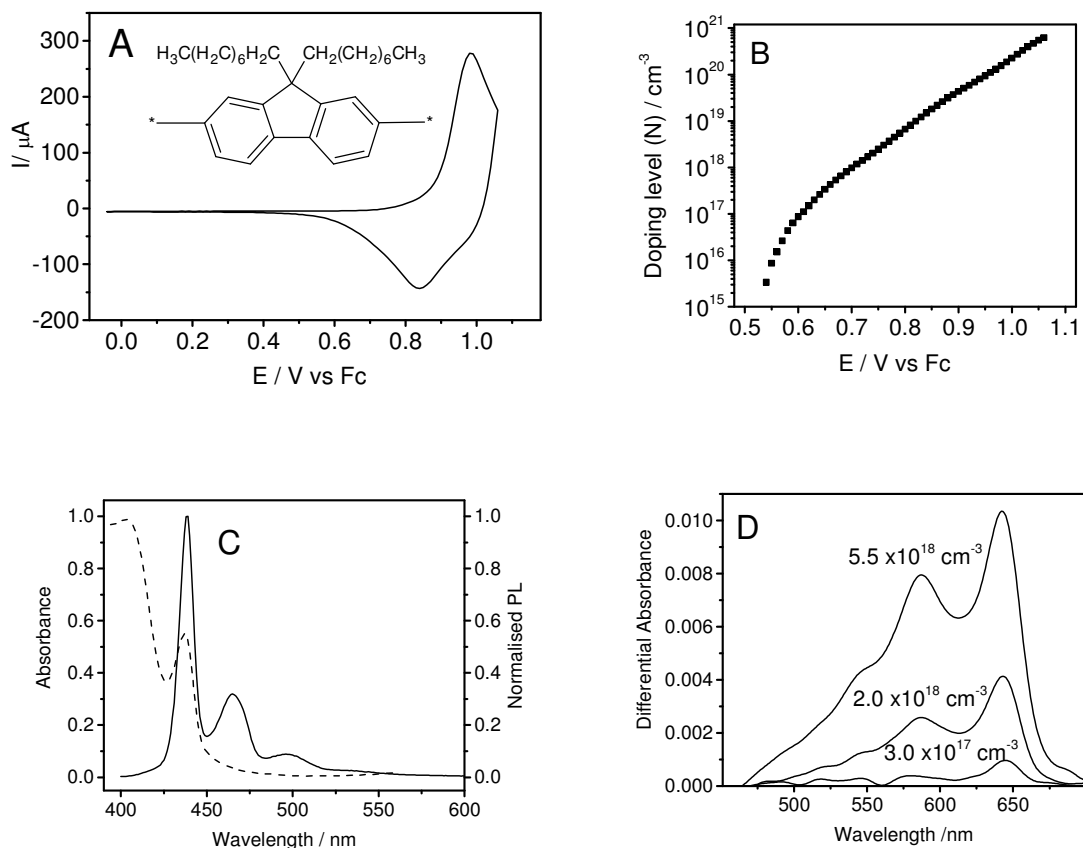


**Figure 1.** (A) Stationary cyclic voltammogram of 50 nm-thick PFO film deposited on ITO electrode recorded at a scan rate of  $100 \text{ mV s}^{-1}$ . (B) Doping level density (hole density per volume) determined as a function of the applied electrochemical potential. (C) Absorbance (dashed line) and photoluminescence spectra (solid line) of undoped PFO film. (D) Electrochemically induced absorbance spectra at different hole densities.

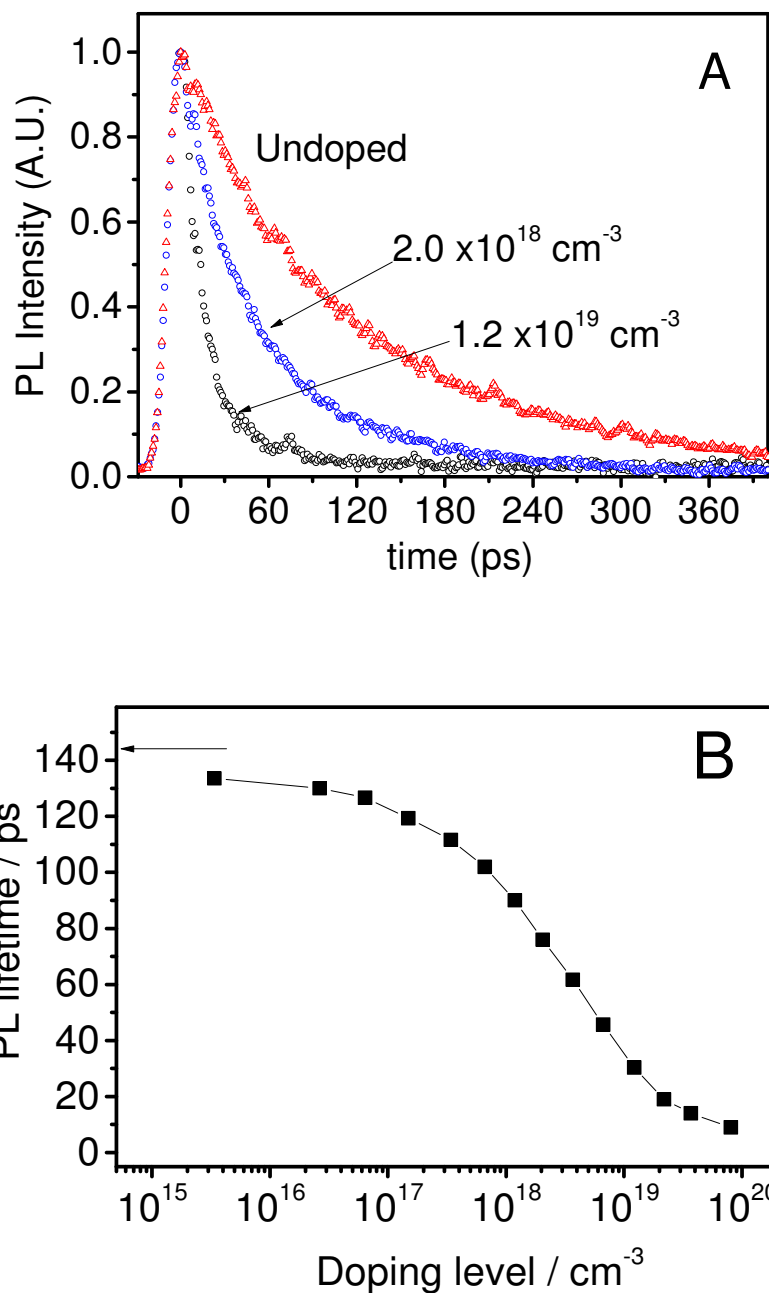


**Figure 2:** (A) Photoluminescence decays in PFO film and at different doping levels (B) Photoluminescence decay time to 1/e of the initial intensity as a function of doping level. The arrow indicates the PL lifetime of the undoped polymer.

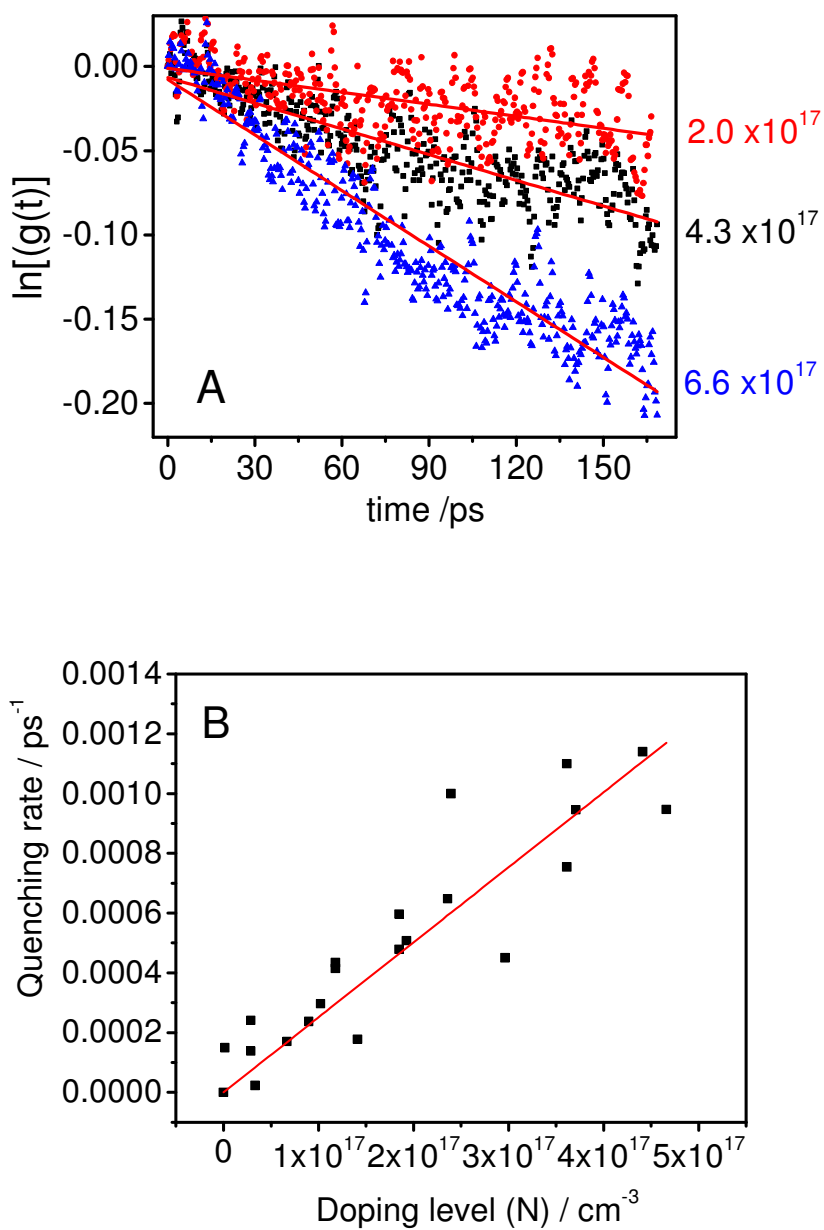


**Figure 3.** (A) Natural logarithm of the PL ratio at selected low charge densities given in cm<sup>-3</sup>. Solid lines are linear fits. (B) Quenching rate constant  $k_q$  as a function of the injected electrochemical charge.

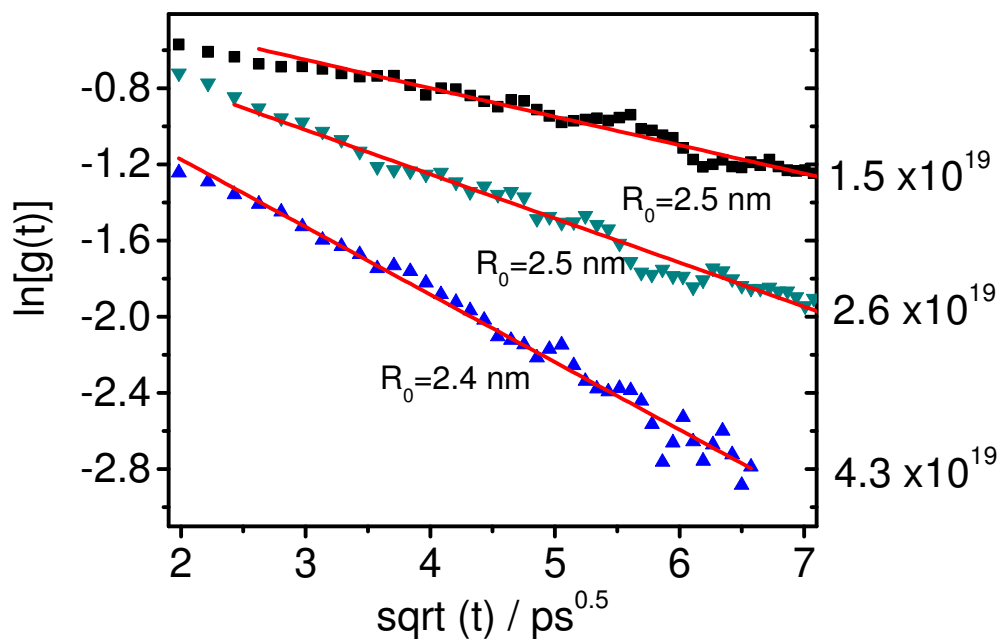


**Figure 4.** Natural logarithm of the PL ratio at high charge densities (in  $\text{cm}^{-3}$ ) plotted vs square root of time. Solid lines are the linear fits. The values of the Förster radius calculated from the fits using Equations (4) and (5) are given next to each curve.

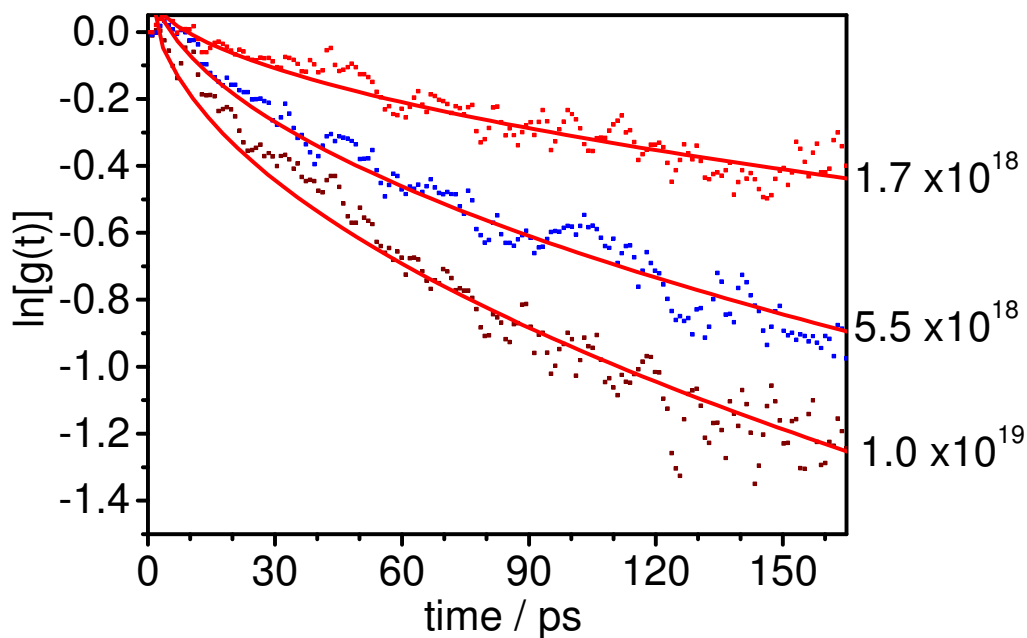


**Figure 5.** Natural logarithm of the PL ratio for PFO at three intermediate charge densities given in units of  $\text{cm}^{-3}$ . Solid lines are fits to Equation (6).

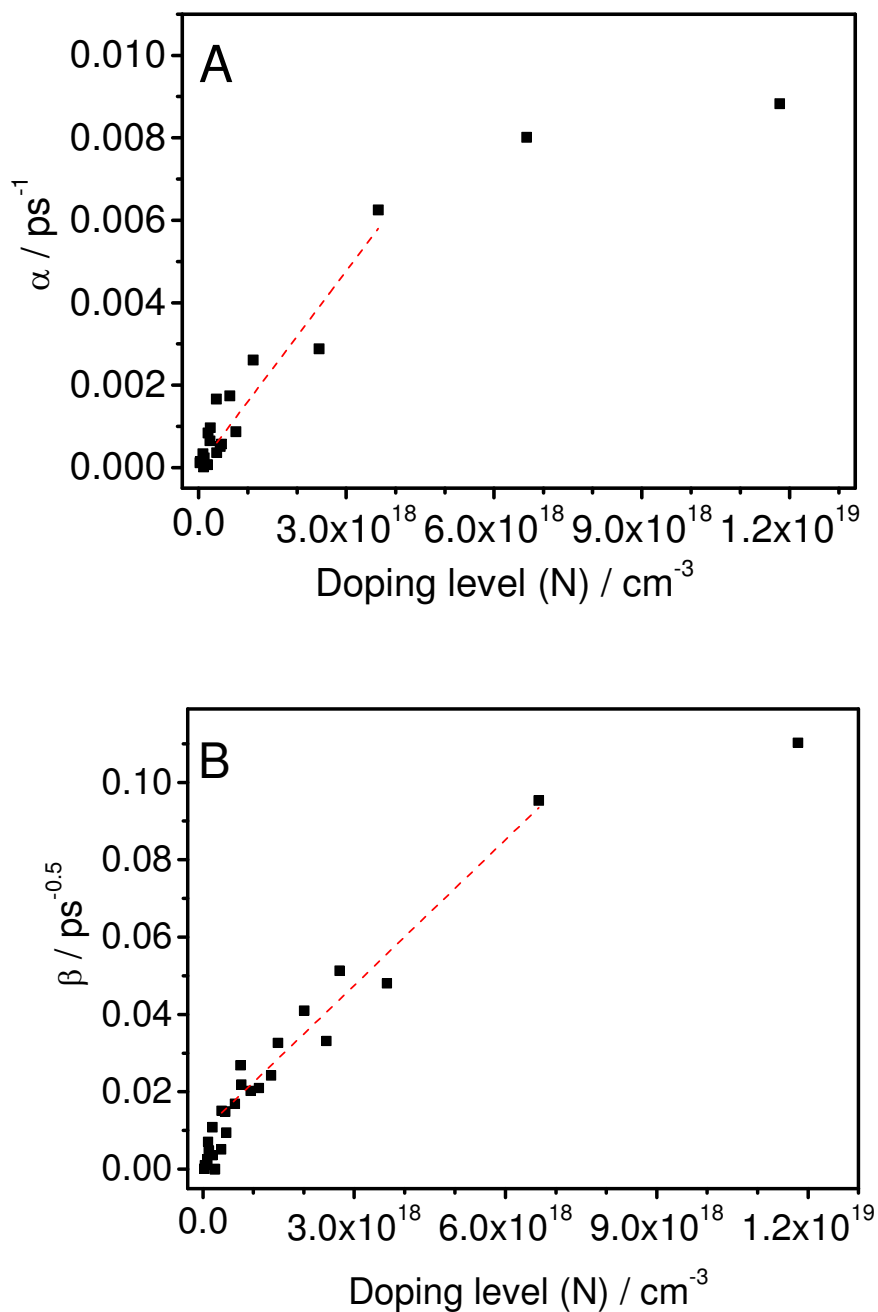


**Figure 6.** (A) Time-independent rate constant of quenching,  $\alpha$ , and (B) time-dependent rate of quenching,  $\beta$ , obtained from the fits to the decays shown in Figure 4. Dashed lines are linear fits.

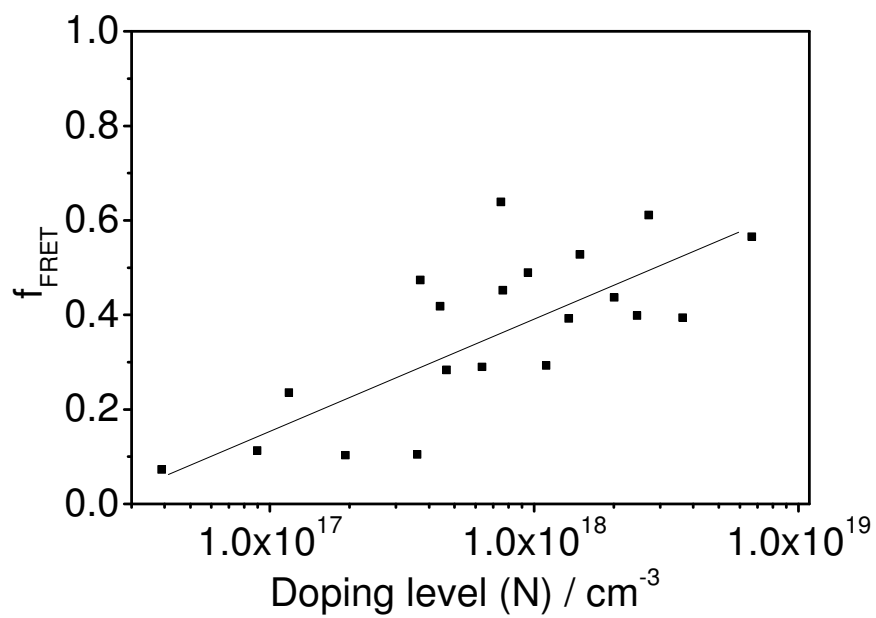


**Figure 7.** Fraction of PL quenching by direct FRET to polaron as a function of doping level.

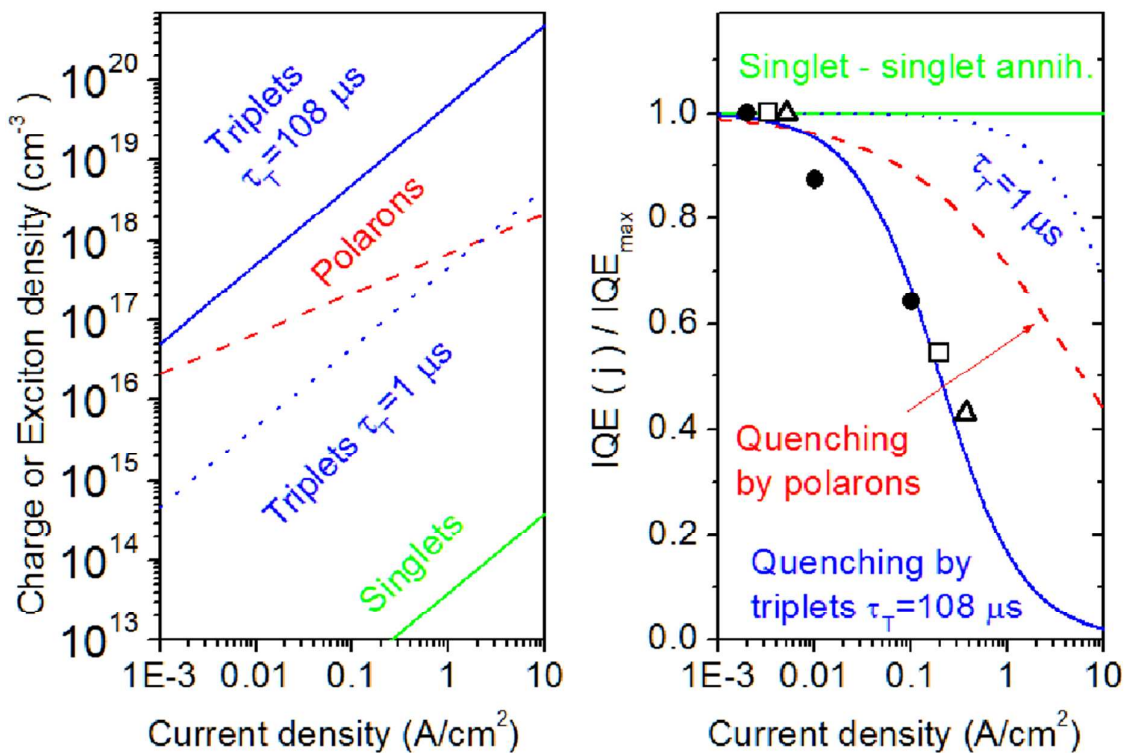


**Figure 8.** (Left) Average density of electron and hole polarons ( $2N$ ) in OLED calculated using Equation (15) (dashed line) and density of singlet and triplet excitons estimated using Equation (16) for different triplet lifetimes  $\tau_T$ . (Right) Normalized internal quantum efficiency calculated using Equations (18) and (19) for different quenching mechanisms of singlet excitons. Symbols are experimental data from ref. <sup>7</sup> (squares), ref. <sup>8</sup> (circles) and ref. <sup>9</sup> (triangles).

## TOC Graphic

